Journal of Power Sources 258 (2014) 365–373

Contents lists available at ScienceDirect

Journal of Power Sources

journal homepage: www.elsevier.com/locate/jpowsour

Optimal charge control strategies for stationary photovoltaic battery systems

Jiahao Li*, Michael A. Danzer

Zentrum für Sonnenenergie-und Wasserstoff-Forschung Baden-Württemberg, Lise-Meitner-Str. 24, 89081 Ulm, Germany

HIGHLIGHTS

- Optimal charge control strategies for PV battery system are mathematically defined.
- Charging performance with two exemplary days and annual profiles are analyzed.
- A multi-objective function is proposed to take all optimization goals into account.
- Battery lifetime is prolonged by minimizing the dwell time at high states of charge.
- Curtailment of PV peak powers is minimized by optimal storage capacity planning.

ARTICLE INFO

Article history:
Received 16 December 2013
Received in revised form
10 February 2014
Accepted 17 February 2014
Available online 25 February 2014

Keywords:
Photovoltaic storage system
Lithium-ion battery
Energy management
Dynamic programming
Charge control
Self-consumption

ABSTRACT

Battery systems coupled to photovoltaic (PV) modules for example fulfill one major function: they locally decouple PV generation and consumption of electrical power leading to two major effects. First, they reduce the grid load, especially at peak times and therewith reduce the necessity of a network expansion. And second, they increase the self-consumption in households and therewith help to reduce energy expenses. For the management of PV batteries charge control strategies need to be developed to reach the goals of both the distribution system operators and the local power producer. In this work optimal control strategies regarding various optimization goals are developed on the basis of the predicted household loads and PV generation profiles using the method of dynamic programming. The resulting charge curves are compared and essential differences discussed. Finally, a multi-objective optimization shows that charge control strategies can be derived that take all optimization goals into account.

1. Introduction

Incentivized by feed-in tariffs and accelerated through dramatically fallen PV module prices, an increase in decentralized renewable power generation in low voltage distribution grids can be observed worldwide. With this development, technical and stability relevant challenges arise for distribution system operators. Feed-in management and mandatory feed-in power limitation came into effect to reduce the grid load at peak times. At the same time, with falling feed-in tariffs and rising electricity prices, local power producers tend to increase their self-consumption.

Due to a lack of synchronization between solar irradiance and local loads, self-consumption of domestic PV systems is usually limited between 25% and 30% [1]. Increasing self-consumption by reducing the size of the PV installation is also not a desirable choice, as it reduces the share of renewable energy content in the energy mix of the household [2]. A solution to reach both goals is the usage of electrical energy storage systems to buffer solar energy, and therewith temporarily decouple generation and consumption. Lithium-ion batteries are well suited in this application to meet the requirements of long calendar and cycle life with a daily charge and discharge cycle and high energy throughput over the battery's lifetime.

One of the major challenges of this solution remains the smart feed-in management applied to the battery storage system. On one hand, charging and discharging processes of lithium-ion batteries need to be controlled to ensure safe applications. On the other hand, new policies were introduced, e.g. by German Renewable Energy Sources Act (EEG 2012) to avoid the overload of the electric grid in Germany. The feed-in limitation of active power is generally limited to 70% of installed peak power of photovoltaic modules, known as peak shaving. If the installed energy storage system is

* Corresponding author. Tel.: +49 731 9530 537; fax: +49 731 9530 599.
E-mail addresses: jiahao.li@zsw-bw.de, jiahao.li@gmx.de (J. Li).

http://dx.doi.org/10.1016/j.jpowsour.2014.02.066
0378-7753/

funded by the government, the limitation is further reduced to 60%. Several studies have already addressed this broader issue. In Ref. [3] demand side management (DSM) is presented to encourage the consumer to shift the energy use to solar peak times such as midday time. According to [4], an extended active DSM with model predictive control is studied to maximize the use of local PV generation. In this way, the need for investments in networks or power plants could be reduced. From the perspective of the energy storage system, Tan et al. [5] proposed a stochastic approach to optimize the battery size in distribution grids with PV plant. In Ref. [6] a rule-based optimal management algorithm is performed to maximize the utilization of renewable energy sources in distribution grids. Williams et al. [2] describe a delayed charging algorithm, which enables the battery charging between 9:00 and 14:00 in the high irradiation months to reduce the grid injection levels. However, these approaches do not take the battery internal dynamics and energy losses into consideration. Technically, the battery operating strategy is not clearly defined.

Given this gap in the literature, this paper proposes an elaborate control strategy to achieve the defined optimization goals without enlarging the battery size or using DSM. Since the power of PV panels and the household consumption could be predicted to some degree, the battery charging power can deterministically be optimized using dynamic programming (DP). Based on different mathematical formulations of the optimization problem results differ in their charging behaviors. An additional goal, extending the battery lifetime, is also considered in this paper since the algorithm takes the battery aging into account.

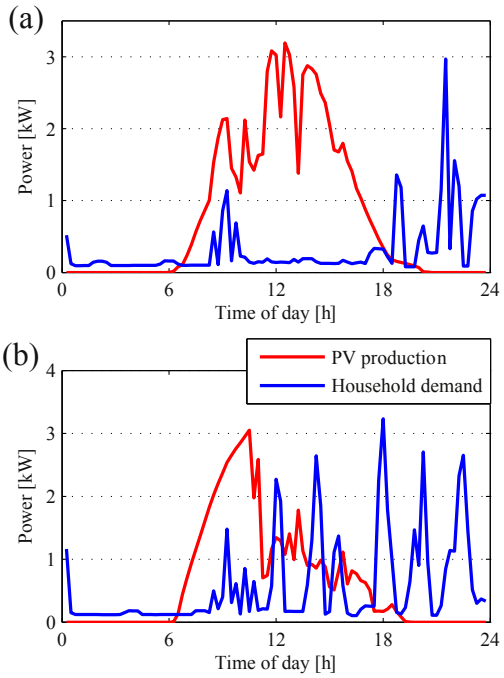

Fig. 2. PV generated power and household loads profiles of two exemplary days with a low (a) and a high (b) correlation of the power demand of the household and solar irradiation, i.e. with a low and high natural self-consumption.

2. Description of the PV battery system

Typical PV systems with integrated battery could be classified as DC coupled and AC coupled power system according to the system configurations. The corresponding DC and AC structures are illustrated in Fig. 1.

In DC coupling energy storage system and PV plants are joined together on the DC side of the system. The battery is connected in the intermediate DC circuit of the PV inverter. In comparison, AC coupled systems join the various power sources on the AC side and the battery is decoupled of the PV inverter. It is notable that in AC coupling energy storage could be retrofitted more flexibly. Batteries are easily integrated into the household independent from the solar installation. Hence AC coupled systems are studied in this work.

The main components of the AC coupled PV battery system are the PV generation, local electrical demand of consumers, distribution grid, and the battery storage system. According to the sign convention, the power balance in the system could be described as the feed-in power

$$P_F(k) = P_{PV}(k) - P_B(k) - P_L(k), \quad \text{when } P_{PV}(k) > P_L(k) \tag{1}$$

and the grid supplied power

$$P_G(k) = P_L(k) - P_{PV}(k) - P_B(k), \quad \text{when } P_{PV}(k) < P_L(k) \tag{2}$$

with k the discrete-time index.

2.1. PV generator and electrical loads

One of the subjects in this paper is to evaluate the self-consumption level of solar energy. It is calculated as the ratio of directly consumed energy to generated PV energy. Therefore, the PV generated profile and household loads should be defined first. These profiles differ from country to country and vary over the

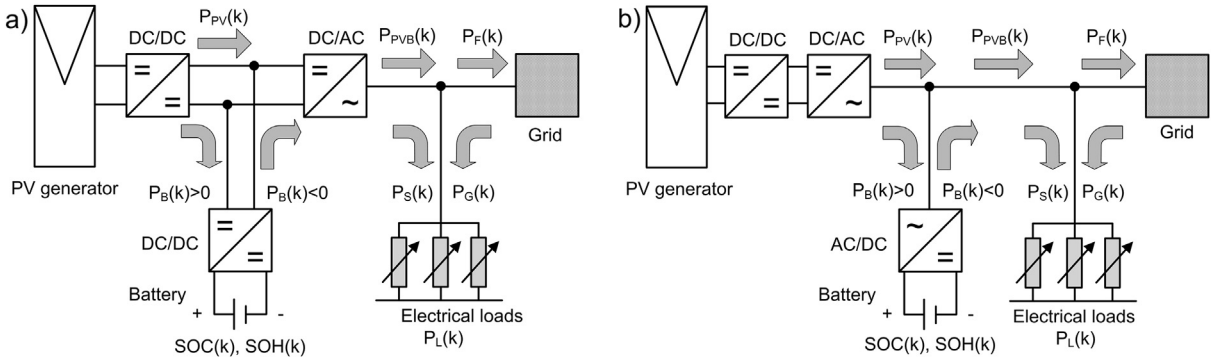

Fig. 1. Schematic illustration of the PV battery systems with power direction and sign convention of PV generated power P_{PV}, battery charge/discharge power P_B, electrical loads P_L, self-consumption P_S, feed-in power P_F, and grid power P_G. (a) Structure of a DC coupled system. (b) Structure of an AC coupled system. Charging the battery from the grid is prohibited.

course of the day, between weekday, weekend and holiday, and the season [7]. In this study, two detailed daily household profiles (see Fig. 2) are considered that are taken from measured data of a four person household with an annual demand of 4000 kWh. As PV power profile the solar irradiation for the location of Stuttgart, Germany, provided by the synthetic weather model of the Software PVSYST with a peak power of 3.5 kW is used. It gains approximately 4000 kWh a^{-1}. Both profiles are depicted in 15-min steps. Therefore, battery charge and discharge profiles are designed for every 15 min. Any faster dynamic in low voltage grid requires an underlying control loop that is not discussed in this article.

2.2. Battery storage system

The battery system accumulates excess energy created by PV plants and supplies the stored energy to the electrical loads when the PV generation cannot cover the local demand. In this paper, a solution with lithium-ion battery is studied, which is currently considered as a particularly promising candidate in distribution grids.

Different mathematical models are used to simulate the electric behavior of a battery. For example, chemical reaction processes can be described by physical and electrochemical equations [8,9]. Equivalent circuit models are commonly used for simulation of the battery voltage and realize a model-based state estimation design [10,11]. In this work, an open-circuit-voltage (OCV) and ohmic resistance based battery model is chosen for the scenario simulation, where OCV can be measured and established as a function of battery SOC. This model is able to take the battery maximum charge/discharge power capability into account and to decrease the computational complexity compared to a dynamic equivalent model with RC circuits. The model structure is shown in Fig. 3.

In general, the battery performance is limited by the battery voltage, allowed SOC, and pulse power capability, which can be summarized as follows:

- Battery voltage

The battery terminal voltage is defined as the summation of the OCV and the dynamic voltage of the ohmic resistance when current flows, as

$$V_{\text{cell},k} = \text{OCV}(\text{SOC}_k) + R_0 \cdot I_k. \tag{3}$$

Experimental results and a simulated discharge curve as a function of discharged capacity are presented in Fig. 4. Using this modeling approach, it is possible to mimic the battery behavior in the applied SOC range.

- Battery state of charge (SOC)

Due to safety, aging, and performance reasons, a typical battery system is operated in a restricted range of SOC, such as 10%–90%. In this application, the current based Coulomb counting law is chosen

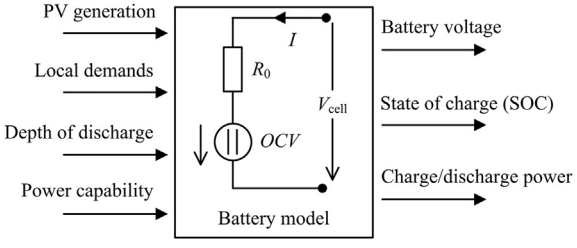

Fig. 3. Inputs and outputs of battery model with open-circuit-voltage OCV and ohmic resistance R_0.

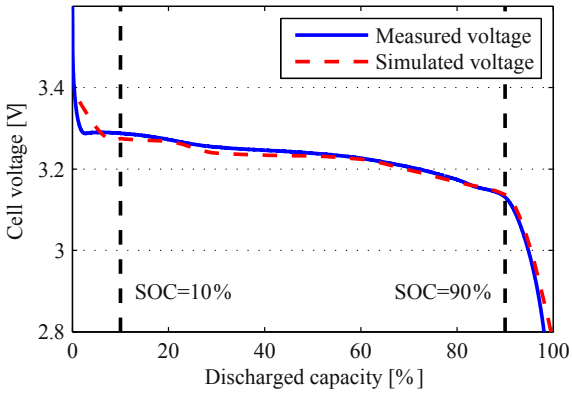

Fig. 4. Comparison of experimental measurement and model-based battery discharge curve at 1C rate. Used SOC range is between 10% and 90% SOC.

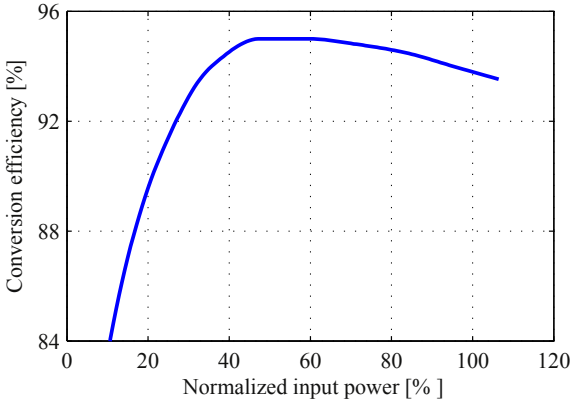

Fig. 5. Conversion efficiency of an inverter with maximum efficiency of 95% around 50% input power.

to determine the battery state of charge. The charge transferred in or out of the battery is obtained by accumulating the current flow over time, which is described as:

$$\text{SOC}_{k+1} = \text{SOC}_k + \eta_c \cdot \frac{I_k \cdot \Delta t}{C_N}, \tag{4}$$

where Δt is the sample time, η_c the Columbic efficiency, C_N is the discharge capacity of the battery and the initial state of charge $\text{SOC}_{k=0} = \text{SOC}_0$.

- Peak power capability

To calculate power capabilities, the hybrid pulse power characterization (HPPC) is used [12], which considers operational limits on battery voltage when estimating available power [13]. With the voltage response expressed by equation (3) and the limits enforced between $V_{\min}$ and $V_{\max}$, the available charge/discharge peak power can be approximately calculated as

$$P^{\text{dis}}_{\text{max},k} = V_{\min} \cdot \frac{(\text{OCV}(\text{SOC}_k) - V_{\min})}{R_0}, \tag{5}$$

and

$$P^{\text{ch}}_{\text{max},k} = V_{\max} \cdot \frac{(V_{\max} - \text{OCV}(\text{SOC}_k))}{R_0}. \tag{6}$$

2.3. Inverter efficiency

As a result of energy transfer, losses are incurred in the power electronics. This part of unusable energy is also considered in this work for the optimal charge control. Inverters usually achieve their maximum efficiency over 95% at around half of the rated output. In Fig. 5 a measured efficiency curve as a function of the input normalized power is shown. This characteristic is applied on the bidirectional AC/DC conversion of the inverters [14].

3. Charge control strategy and system constraints

The idea of controlling the battery charging power is initiated by different operating strategies. Its inputs are the battery parameters, e.g. voltage, SOC, and system constraints. The control strategy makes decisions or regulates the battery current to reach the operating goals.

In general, charge strategies can be optimized towards the interest of the two engaged players: the distribution system operator and the local power producer. For the first group peak shaving or limitation of feed-in gradients are methods to reduce the network load and the power fluctuation in the grid. For local producers optimization might be performed to maximize the self-consumption and therewith to minimize energy expenses. In the following a set of optimization goals are formulated and translated into mathematical objective functions. Above all, it is important to note that a battery is forced to discharge, when the load demand $P_L(k)$ exceeds the PV generation. The battery is discharged, if

$$P_L(k) > P_{\mathrm{PV}}(k). \tag{7}$$

This criterion is valid for all applications.

- Fast charging with excess PV power

Battery storage systems are used to capture excess PV energy. The charging strategy where the battery gets charged as soon as excess PV power is available can be regarded as fast charging. The corresponding charging current is calculated as

$$I_k = \frac{P_{\mathrm{PV},k} - P_{L,k}}{V_k}. \tag{8}$$

As for the optimization design, the objective function

$$J_t = \sum_{k=t_0}^{T} (\mathrm{SOC}_{\max} - \mathrm{SOC}_k) \tag{9}$$

is formulated such that the battery SOC is kept at its maximum state.

- Charging for maximizing battery lifetime

Battery degradation processes take place during operation and also at rest periods where no current is applied. These aging phenomena are studied in Refs. [15,16], based on a superposition of cycle and calendar aging. In this work deep cycle solar batteries with 90% depth of discharge (DoD) are designed to be repeatedly discharged and recharged for daily applications. Due to the fixed battery DoD, optimization of battery cycling has a comparatively low impact on the degradation process. In comparison, reduced dwell times at the fully-charged state increases the lifetime of most Li-ion based battery types. In addition, the capacity decrease with increase in storage time and temperature are expected. A battery calendar aging model from [17] is applied as the objective function for this application

$$J_{\mathrm{cal}} = \sum_{k=t_0}^{T} \left(A_0 \cdot \exp\left(\frac{\mathrm{SOC}_k - \mathrm{SOC}_r}{b}\right) \cdot \exp\left(\frac{T_k - T_r}{c}\right) \cdot \left(\sqrt{t_k} - \sqrt{t_{k-1}}\right)\right), \tag{10}$$

where the calendar aging is proportional to the root of the time. A_0 in equation (10) corresponds to the nominal lifetime, while the cell is kept at the reference states $\mathrm{SOC_r}$ and temperature T_r. An exponential dependency of the aging on battery SOC_k and temperature T_k is observed. It is assumed that a doubled aging rate occurs with a temperature rise of 15 K and an increase of the SOC by 40% [17]. Thus b in equation (10) is chosen as $0.4/(\log\sqrt{2})$ and c as $15/(\log\sqrt{2})$. Since the operating temperature for all analyzed charging scenarios is kept constant at room temperature (23 °C) the effect of temperature on battery aging is not taken into account in this study.

- Charging for maximizing self-consumption (SC)

With degressive feed-in tariffs and rising electricity prices, PV generated solar energy is considerably more attractive when it is self-consumed rather than being sold. In households, self-consumption is defined as the ratio of locally used, self generated electricity to the total PV energy

$$\mathrm{SC} = \frac{\int P_{\mathrm{PV}}\mathrm{d}t - \int P_F \mathrm{d}t}{\int P_{\mathrm{PV}}\mathrm{d}t}. \tag{11}$$

To design an optimal charge control strategy, the aim of maximizing self-consumption needs to be reformulated as a minimization problem to

$$J_{\mathrm{sc}} = \sum_{k=t_0}^{T} \left(\underset{P_{F,k}(\Delta t)>0}{P_{F,k} \cdot \Delta t} \right), \tag{12}$$

where the feed-in energy is minimized.

- Charging for maximizing self-sufficiency (SS)

Apart from the self-consumption level, self-sufficiency is another important characteristic evaluating the grid integration. Self-sufficiency is defined as the ratio of domestic load not supplied by the grid to the total domestic load

$$\mathrm{SS} = \frac{\int P_L \mathrm{d}t - \int P_G \mathrm{d}t}{\int P_L \mathrm{d}t}. \tag{13}$$

The major difference between self-sufficiency and self-consumption is that losses of PV power due to inverters and batteries will lower SS where they increase SC. High levels of self-sufficiency can be achieved when only a small amount of energy is supplied from the distribution grid. Accordingly, the objective function can be expressed as a minimum power supplied by the grid

$$J_{ss} = \sum_{k=t_0}^{T} \left(\underset{P_{G,k}(\Delta t)>0}{P_{G,k} \cdot \Delta t} \right), \tag{14}$$

with the definition of $P_{G,k}$ in equation (2).

- Charging for cost minimization

For private households the control objective is to lower the energy costs while satisfying the grid feed-in constraints. This can be further formulated as a cash-flow function considering cash gained from feed-in and cash paid for electricity from the grid

$$J_c = -\sum_{k=t_0}^{T} \left(\underset{P_{F,k}(\Delta t)>0}{P_{F,k} \cdot \Delta t \cdot FiT} - \underset{P_{G,k}(\Delta t)>0}{P_{G,k} \cdot \Delta t \cdot Ep} \right), \tag{15}$$

where Δt is the discrete time step, Ep the electricity price per kWh, and FiT the feed-in tariff. It is notable that compared to equation (12) the overall energy expense can be optimized in equation (15), since battery charging efficiency at different operating points is considered and energy loss is thus reduced at the battery charging process.

- Multi-objective optimization

Multi-objective optimization algorithms allow for optimizations that contain multiple objective functions simultaneously [18]. Each objective can be a minimization or a maximization of the outputs equations (9)–(15). When objectives are conflicting with each other in the case of J_t and J_{cal}, J_{sc} and J_c, some trade-off between the criteria is needed to ensure a satisfactory design.

For the sake of optimal charging, the battery lifetime and energy costs are more attractive for private users on the premise that maximum grid injections are limited first. Therefore, a possible objective function can be formulated as the superposition of J_{cal} and J_c

$$J_m = q \cdot J_{cal} + r \cdot J_c, \tag{16}$$

where q and r are weighting factors.

Following the optimization functions, the operating range of the system components is limited. Boundary conditions have to be set on the SOC range, battery voltage, charging/discharging power, maximum feed-in power and power gradient. To summarize, the constraints for the battery are defined as

$$SOC_{min} \le SOC_k \le SOC_{max}, \tag{17}$$

$$V_{min} \le V_k \le V_{max}, \tag{18}$$

and

$$P_{max,k}^{dis} \le P_{B,k} \le P_{max,k}^{ch}, \tag{19}$$

where battery state of charge and voltage should remain in constant, predefined ranges for reasons of safety and aging, and the battery power is limited dynamically to its current power capabilities P_{max}^{dis} and P_{max}^{ch}. The constraints for the grid feed-in are a maximum feed-in power and a maximum feed-in gradient

$$P_{F,k} \le P_{F,max}, \tag{20}$$

and

$$\frac{dP_{F,k}}{dt} \le p_{F,max}. \tag{21}$$

Therefore the objective function of equation (16) takes the interests of household into account. The interests of the grid are implemented as constraints in equations (20) and (21) and are not allowed to be violated during operation.

4. Methodology of dynamic programming

The defined nonlinear minimization problem is incorporated into an optimization design, known as dynamic programming. It is a method for solving the complex optimization problem by identifying a collection of subproblems. The DP algorithm was firstly proposed by Richard Bellman in 1957 [19]. To calculate this optimal control sequence, a discrete system model is applied.

Note that the system sample time is fixed as Δt in equation (4). In this interval the battery SOC_k is kept constant, with a step size of ΔSOC. The discrete samples are indexed by the variable $k = [1,\ldots,N]$ with

$$N = \frac{T}{\Delta t} \tag{22}$$

defined by the length of the optimization period T. In addition, the battery charging/discharging power $P_{B,k}$ is considered as a discrete control level. The value is mapped onto a fixed grid with distance ΔP_B, such that exactly $m + 1$ power levels are utilized [20], with

$$m = \frac{P_{max,k}^{ch} - P_{max,k}^{dis}}{\Delta P_B}. \tag{23}$$

After discretization, the optimization problems formulated in the previous section can be regarded as a multistep decision problem. Let $\pi = \{P_{B,0}, P_{B,1}, \ldots P_{B,N-1}\}$ be a control sequence. At each time instant, the battery charging power has to be decided for the next time interval, which achieves the smallest objective value J^o over a certain trajectory π [20], expressed as

$$J_\pi(SOC_0) = \phi_N(SOC_N) + \sum_{k=0}^{N-1} \phi_k(SOC_k, P_{B,k}), \tag{24}$$

and

$$J^o(SOC_0) = \min_{\pi \in \Pi} J_\pi(SOC_0), \tag{25}$$

where ϕ_N is the end cost, ϕ_k the cost of applying the control signal $P_{B,k}$, and Π the set of all admissible trajectories.

Based on the principle of optimality [19], the DP algorithm evaluates the optimal cost-to-go function J_k^* at each time instant by proceeding backwards in time [21]:

1) End cost calculation step

$$J_N^*\left(SOC_N^*\right) = \phi_N\left(SOC_N^*\right), \tag{26}$$

2) Intermediate calculation step for $k = N - 1$ to 0

$$J_k^*\left(SOC_k^*\right) = \min\left\{\phi_k\left(SOC_k^*, P_{B,k}\right) + \ldots + J_{k+1}^*\left(SOC_{k+1}^*\right)\right\}, \tag{27}$$

where * describes the optimal value of the subproblem at time step k. Fig. 6 illustrates the output of the algorithm equations (26) and (27) as an optimal control signal map. This map is used to find the optimal control signal during a forward simulation of the model

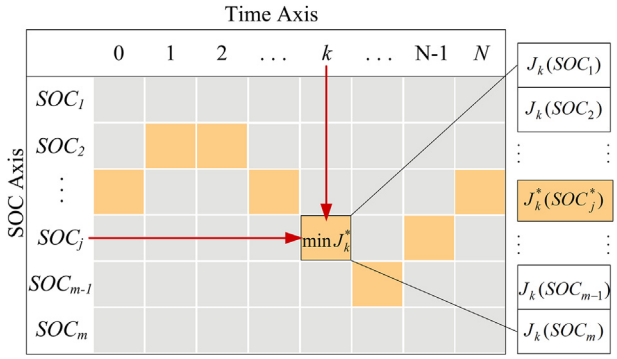

Fig. 6. A possible SOC trajectory minimizing a cost function with the optimal value J_k^* at time step k.

equation (4), starting from a given initial state SOC_0 to generate the optimal state trajectory.

To perform the optimal charge control methodology, a flowchart is presented in Fig. 7. The input parameters are the PV generation and electrical loads of one day at 15-min intervals. At each time step k, the DP algorithm is executed with all discretized SOC values. Therefore, all possible charge trajectories from the initial SOC at the start of the day to the allowed battery states at the end of the day are evaluated. The sequence of SOC with the minimum value of the objective function is considered as the optimal battery charge curve.

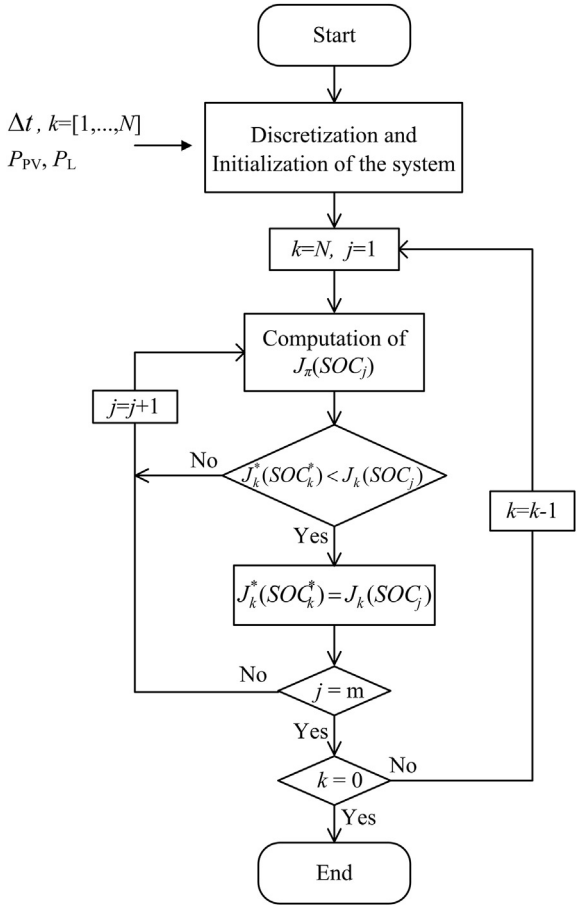

Fig. 7. Proposed structure of DP procedure for the optimal charge control.

4.1. System definition

In the following, all necessary parameters are given for the DP design. With respect to a household standard, a simulated $LiFePO_4$ as cathode and graphite as anode battery system with an energy of 3.3 kWh is used to increase the self-consumption level. The energy storage system is composed of 10 cells, with an ohmic resistance of 3 mΩ per cell. Additionally, the grid limitation of feed-in is defined, which contains information about the peak power shaving and the power gradient per unit time. Other relevant configurations such as feed-in tariff, electricity price, and system constraints in equations (17)–(21) are detailed in Table 1.

5. Simulation results and discussion

5.1. Scenarios of two exemplary days

For the purpose of comparing the various optimal charge control strategies, simulations have been carried out with load profiles of two exemplary days. Battery charging curves and the corresponding feed-in power are detailed in Fig. 8, where the day with a low correlation of the household consumption and solar irradiation is shown. At the beginning an initial SOC of 10% is chosen. SOC upper limit is set to 90%. Charging behavior with excess PV power is shown in Fig. 8(a). As expected, the battery is charged with the first available power to its maximum level. The storage capacity is exploited before the PV peak production which leads in consequence to a curtailment to obey the feed-in limitation. By comparison the charging curve for 'maximizing lifetime' is shown in Fig. 8(b). Based on the predicted demand profile, the charging process is not directly initiated in the morning as there is a midday period with more PV energy. The battery SOC reaches the fully-charged state at the last possible charging period. No curtailment is required.

Fig. 8(c) illustrates subsequently the charging curve for increasing self-consumption. Note that this result differs from the one in Fig. 8(e), in which the cash-flow is optimized by maximizing the entire feed-in energy. Under the circumstances that PV power is in priority used to supply the local demands, the total energy loss in the power electronics is reduced in Fig. 8(e). In this case, the battery is charged only when PV excess power is sufficient to achieve higher inverter efficiency mainly at midday period.

Fig. 8(d) depicting maximization of self-sufficiency performs a similar charging algorithm as in Fig. 8(a). But the energy storage is operated such that future local demands are fulfilled. Due to the

Table 1
Overview of the studied system for DP design.

Battery specification	
Nominal capacity	100 Ah
Ohmic resistance	3 mΩ
Number of batteries in series	10
Operational voltage	27 V–38 V
Operational SOC	10%–90%
Max. charging/discharging power	3 kW
Grid constraints and electricity cost	
Feed-in power	60% of installed PV peak power
Power gradient	2.5% per minute
Feed-in tariff	16 €ct kWh^{-1}
Electricity price	30 €ct kWh^{-1}
Simulation configurations	
SOC discretization	0.1%
Start SOC	10%
End SOC	Free, max 90%
Period of optimization	24 h
Time step	15 min

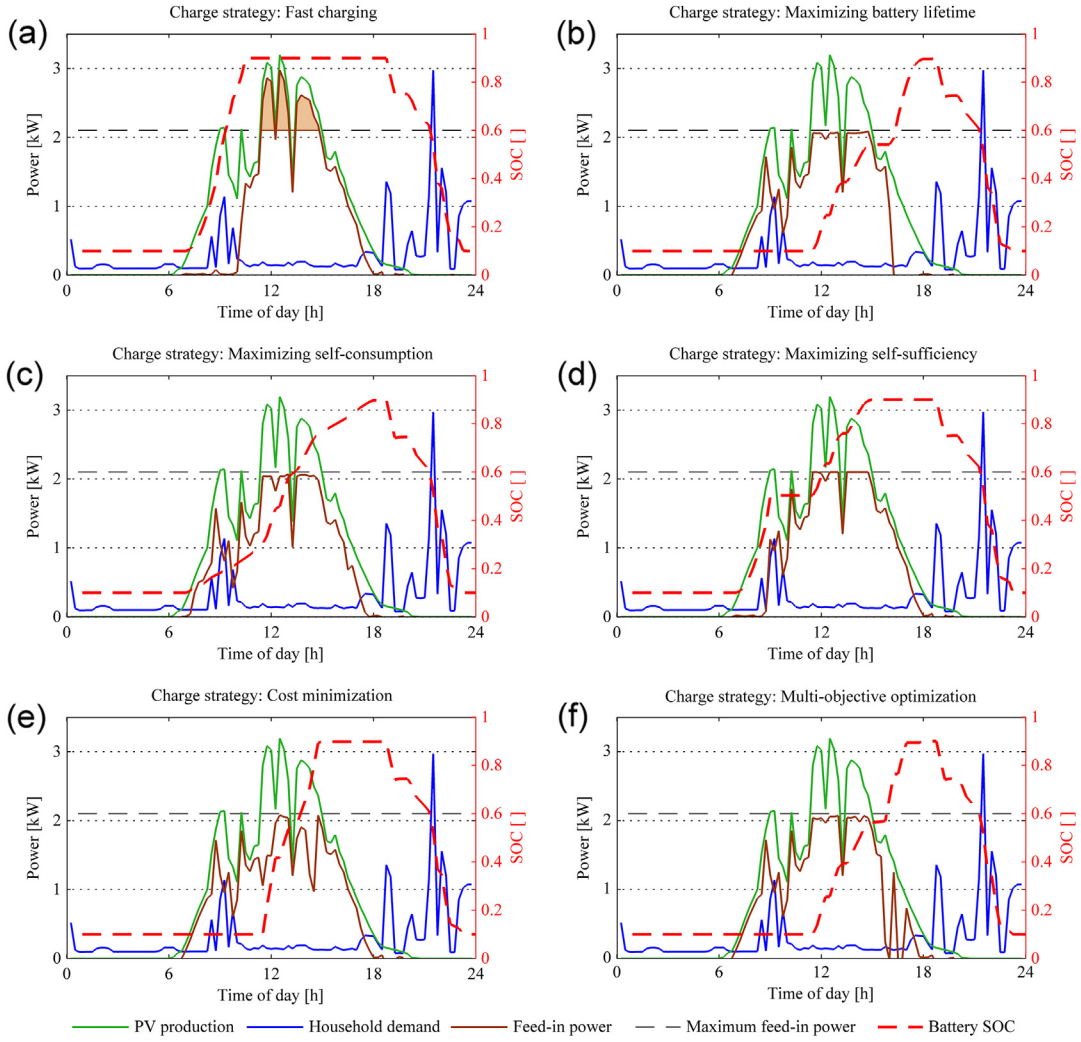

Fig. 8. Results of all charge control strategies for day 1 with feed-in limitation of $P_{F,max}$ = 2100 W. Filled areas are lost PV generation through curtailment.

system constraints of feed-in limitation, the battery charging is shortly interrupted to capture the PV peak production.

Concerning the above information a multi-objective optimization is applied in Fig. 8(f), where the tuning parameters in equation (16) are chosen to be equal. The battery is charged comparatively late in the day. More detailed information is shown in Table 2.

In Fig. 9 the load profile of the second day is employed. Results depict the charging performance with fast charging strategy and the multi-objective optimization. In this case, due to an alignment between demand and PV generation, self-consumption is significantly improved. In Fig. 9(b) additional benefits can be achieved when the battery is partially discharged and recharged to 90% rather than remaining at the high state of charge.

An overview of the charging behaviors in terms of cash-flow, self-consumption, and self-sufficiency is presented in Table 2. Generally, the advantages of the energy storage system are obvious. At both days levels of SC and SS are increased. Considering various objective functions within DP design, the resulting charging strategies are further validated. As mentioned before, the battery should be primarily discharged when the domestic load is higher than the PV production (see equation (7)). This leads to an almost identical SS level for all strategies as shown in the table. The variations in cash-flow and SC are mainly because of the extra losses from the battery and inverters. In contrast, due to the feed-in limitation and the consequent curtailment the cash flow with fast charging strategy is significantly lower than for the other cases.

Table 2
Comparison of various charging strategies in terms of cash-flow, self-consumption, and self-sufficiency with positive values for cash gained and negative values for cash paid.

Charging strategies (feed-in limitation)	1st day with low natural SC.			2nd day with high natural SC.		
	Cash-flow (€)	SC (%)	SS (%)	Cash-flow (€)	SC (%)	SS (%)
Without storage (70%)	+0.83	17.4	39.5	−1.05	34.2	34.7
Fast charging (60%)	+1.18	31.5	69.4	−0.76	61.9	61.2
Min. aging (60%)	+1.54	31.6	69.2	−0.64	61.8	60.9
Cost optimization (60%)	+1.56	30.9	69.6	−0.62	61.6	61.5
Self-consumption (60%)	+1.47	33.4	69.7	−0.69	64.2	61.3
Self-sufficiency (60%)	+1.53	31.5	69.7	−0.65	61.9	61.5
Multi-objective (60%)	+1.55	31.1	69.6	−0.63	61.6	61.3

5.2. Scenarios of annual PV and demand profiles

In this section, annual PV and demand profiles are loaded in series to evaluate the charging performance with the multi-objective optimization algorithm. Fig. 10 illustrates a histogram

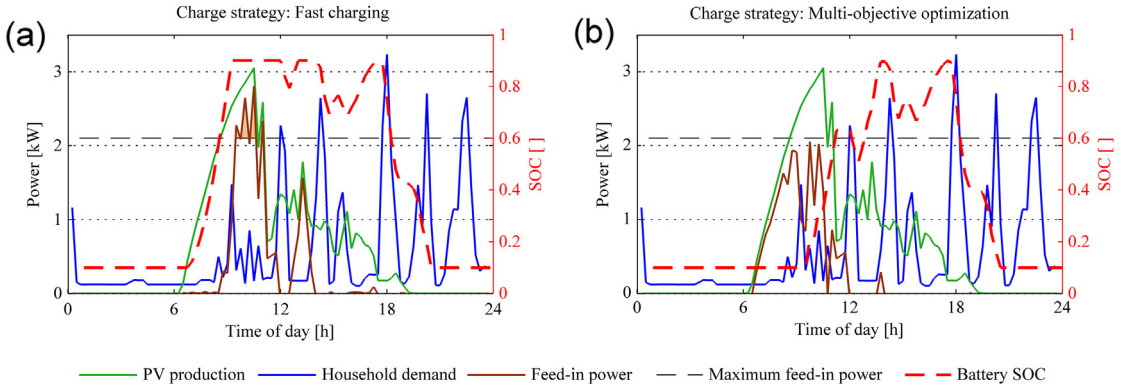

Fig. 9. Comparison of charging performance with fast charging (a) and the multi-objective optimization (b) for day 2. Filled areas are lost PV generation through curtailment.

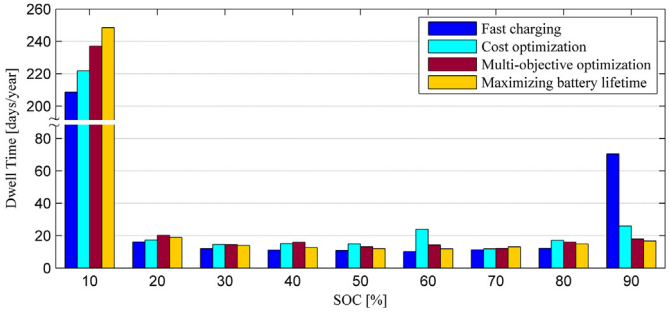

Fig. 10. Distribution of battery dwell time at different SOC ranges.

for the distribution of battery dwell time at different SOC ranges. It is evidently shown that through the multi-optimization strategy the dwell time at high states of charge (>85% SOC) are reduced from 70 days year^{-1} to 19 days year^{-1}. On the basis of the mean battery SOC, the calendar aging rates with various control strategies are depicted in Fig. 11. The battery's state of health (SOH) as a function of SOC can be expressed as

$$\mathrm{SOH} = 1 - \sum J_{\mathrm{cal}}, \tag{28}$$

where the nominal battery calendar life at 50% SOC is assumed to be 10 years. SOH in equation (28) is 1 at begin of life (BOL) and 0 at end of life (EOL) which is defined as 20% capacity loss related to the initial capacity value. It is notable that the average SOC levels in Fig. 10 are far below the reference value, the calendar lifetime is thus extended to approximately 15 years in Fig. 11. As a second consequence, an extension of the lifetime improves the total cost of ownership (TCO) of the energy storage system.

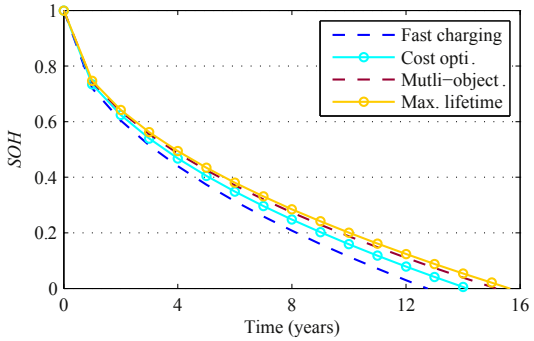

Fig. 11. Effect of the optimization strategy on the calendar aging of the battery.

Based on the balance of cash paid and cash gained in equation (15), the annual energy expenses with different methods are consequently calculated. Results are shown in Fig. 12. Note that the electricity costs are very dependent on the pricing scenarios. Due to a lower feed-in tariff, a significant reduction in energy costs can be obtained with the energy storage system. In the optimal case, cash paid based on the cost optimization with 312 € is over 10% lower than the standard fast charging method with 352 €. Similar benefit can be further guaranteed with a multi-optimization charging with 318 € per year. To conclude, using the multi-objective function the battery lifetime is prolonged while the economic benefits offered through the storage system are maximized.

In Fig. 13 the overall effects on the grid injection with the multi-objective algorithm in comparison to fast charging is displayed. Feed-in scenarios as percentage values of installed PV peak power (3.5 kWp in this work) over the year are shown. The corresponding annual injection curves along with the cumulated hours per year are shown in Fig. 14. As expected, the battery capacity with fast charging is fully used in the early hours of the day. In contrast, multi-objective optimized battery charging exhibits a strategic improvement. The battery is charged rather at the afternoon periods. Therefore, fluctuation over the feed-in limitation is able to be entirely accommodated with the storage system.

6. Conclusion

In this work predictive charge control strategies for stationary PV battery systems based on dynamic programming are presented. For the optimization design the study focuses on the various charging goals formulated as the objective functions in Section 3. Comparison in Table 2 shows that maximizing the PV self-

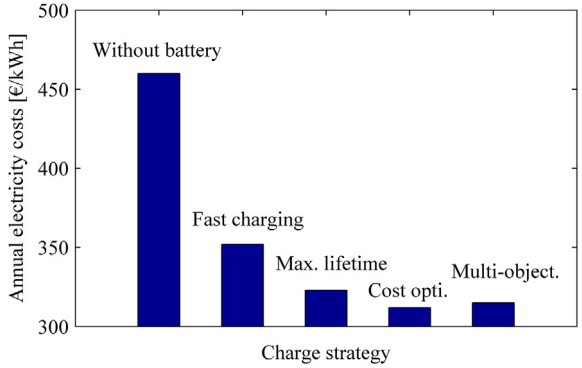

Fig. 12. Comparison of annual electricity costs.

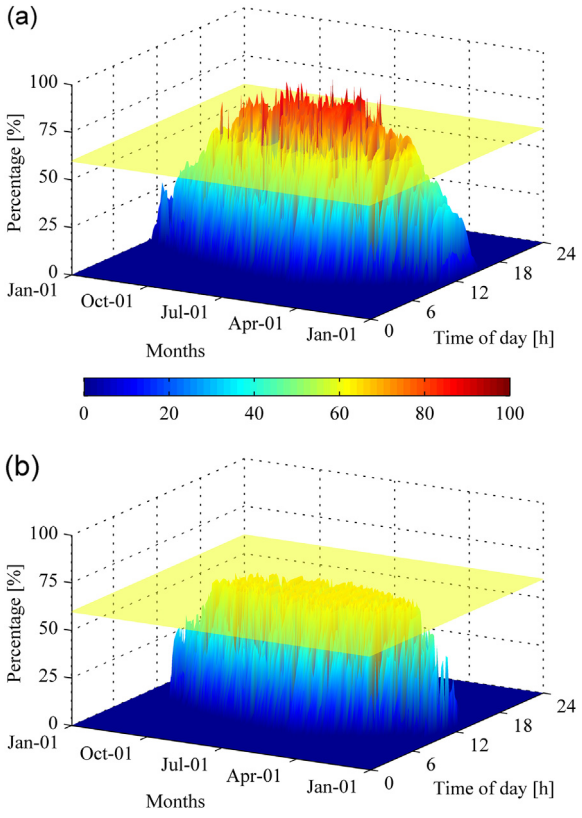

Fig. 13. PV injection levels into the grid with fast charging (a) and multi-objective optimization (b). PV generation above the yellow plane in (a) are lost due to curtailment. For the multi-objective optimization no curtailment occurs. (For interpretation of the references to color in this figure legend, the reader is referred to the web version of this article.)

consumption may not be the best way to manage a battery pack, as more energy is lost during the power flow. Considering the battery lifetime and economic factors for local power producers, battery charging in a multi-objective optimization is investigated. The key characteristics of the approach are:

- reduction of the PV injection and smoothing of the feed-in power into the grid without enlarging the battery size,
- battery lifetime is prolonged by minimizing the dwell time at high states of charge,
- losses are minimized by operating the PV battery at high inverter efficiencies, and
- optimization of electricity costs with DP design is simultaneously guaranteed.

The optimization anticipates PV peak production and local demands. In real conditions, the efficiency of the predictive schedule

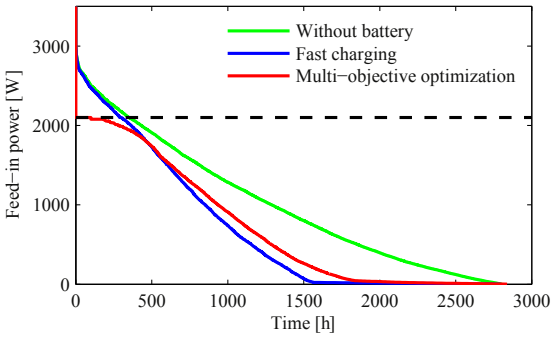

Fig. 14. Annual grid injection duration curves for the various cases with the dashed line presenting the feed-in limitation. A levelizing effect of the multi-objective optimization can be seen: feed-in occurs mainly at low power levels.

depends on the accuracy of the irradiation and local load forecast that can be supported by Markov-Chain Monte Carlo methods, human behavior simulation, and learning methods. The presented algorithm is well suited for a globally optimal storage capacity planning over the course of one day.

References

[1] V. Wachenfeld, in: 5th IRES, 2010. Berlin, Germany.
[2] C. Williams, J. Binder, T. Kelm, in: 3rd ISGT, 2012. Berlin, Germany.
[3] M. Castillo, A. Gutierrez, F. Monasterio-Huelin, E. Caamano, D. Masa, J. Jimenez-Leube, Energy Convers. Manage. 52 (2011) 2659–2666.
[4] Y. Zong, in: IEEE ISGT Europe, 2012, pp. 1–8. Berlin, Germany.
[5] C. Tan, T. Green, C. Hernandez-Aramburo, Energy 35 (2010) 5082–5092.
[6] A. Purvins, M. Sumner, J. Power Sources 242 (2013) 742–755.
[7] A. Purvins, Ioulia T. Papaioannou, L. Debarberis, Energy Convers. Manage. 65 (2013) 272–284.
[8] K.A. Smith, C.D. Rahn, C.Y. Wang, in: IEEE CCA, 2008, pp. 714–719. San Antonio, USA.
[9] P. Arora, M. Doyle, R.E. White, J. Electrochem. Soc. 146 (1999) 3543–3553.
[10] Gregory L. Plett, J. Power Sources 134 (2004) 262–276.
[11] J. Li, J.K. Barillas, C. Guenther, M.A. Danzer, J. Power Sources vol. 230 (2013) 244–250.
[12] FreedomCAR Battery Test Manual for Power-Assist Hybrid Electric Vehicles, 2003.
[13] G.L. Plett, IEEE Trans. Veh. Technol. 53 (2004) 1586–1593.
[14] Y. Riffonneau, S. Bacha, F. Barruel, S. Ploix, IEEE Trans. Sustainable Energy 2 (2011) 309–320.
[15] R.B. Wright, C.G. Motloch, J.R. Belt, J.P. Christophersen, C.D. Ho, R.A. Richardson, I. Bloom, S.A. Jones, V.S. Battaglia, G.L. Henriksen, T. Unkelhaeuser, D. Ingersoll, H.L. Case, S.A. Rogers, R.A. Sutula, J. Power Sources 110 (2002) 445–470.
[16] M. Ecker, N. Nieto, S. Käbitz, J. Schmalstieg, H. Blande, A. Warnecke, D.U. Sauer, J. Power Sources 248 (2014) 839–851.
[17] C. Guenther, B. Schott, W. Hennings, P. Waldowski, M.A. Danzer, J. Power Sources 239 (2013) 604–610.
[18] R. Dufo-Lopez, J. Bernal-Agustin, J. Yusta-Loyo, J. Dominguez-Navarro, I. Ramirez-Rosado, J. Lujano, I. Aso, Appl. Energy 88 (2013) 4033–4041.
[19] R. Bellman, Dynamic Programming, Princeton University Press, Princeton, 1957.
[20] M. Koot, J. Kessels, B. de Jager, W. Heemels, P. van den Bosch, M. Steinbuch, IEEE Trans. Veh. Technol. 54 (2005) 771–782.
[21] O. Sundström, L. Guzzella, in: IEEE Multi-Conference on Systems and Control, 2009, pp. 1625–1630.